Ueda and Kato
Progress in Earth and Planetary Science (2023) 10:31
https://doi.org/10.1186/s40645-023-00564-0

Progress in Earth and Planetary Science

RESEARCH ARTICLE

Open Access

Aftershocks following the 2011 Tohoku-Oki earthquake driven by both stress transfer and afterslip

Taku Ueda[1*] and Aitaro Kato[2]

Abstract

Aftershocks are a fundamental characteristic of seismicity, and their generation mechanism is mainly characterized by two physical models, stress transfer from large earthquakes and afterslip-induced stress loading. However, the contribution of each mechanism to aftershock generation remains unclear. Here we investigate the spatiotemporal variations in aftershock activity following the 2011 Tohoku-Oki earthquake by applying the Hierarchical Space–Time Epidemic-Type Aftershock Sequence (HIST-ETAS) model to the decade of recorded seismicity since the mainshock. Using the estimated HIST-ETAS model, we categorize the aftershocks into background earthquakes (which are caused by aseismic phenomena) and triggered earthquakes (which are caused by earthquake-to-earthquake interactions). Most of the earthquakes that occurred updip of the large coseismic slip zone along the Japan Trench are triggered earthquakes, consistent with the lack of afterslip in this area. Conversely, background earthquakes are the predominant earthquake type in the long-term downdip of the large coseismic slip zone, and they positively correlate with the afterslip evolution. Our results suggest the importance of combining these two end-member aftershock generation models to explain aftershock activity and thus provide new insights into the relationship between afterslip and spatiotemporal aftershock distribution. Our classifications may also contribute to the monitoring of afterslip in a given region that hosts a large earthquake, particularly where geodetic observation networks are too sparse to evaluate afterslip evolution.

Keywords Aftershock, Stress transfer, Afterslip, 2011 Tohoku-Oki earthquake, HIST-ETAS model, Background earthquakes, Triggered earthquakes

1 Introduction

The 2011 M9 Tohoku-Oki earthquake occurred on March 11, 2011, along the boundary between the subducting Pacific Plate and the overriding Okhotsk Plate (Fig. 1). Previous studies reveal the aftershock distribution in and around the focal area of this megathrust earthquake (e.g., Asano et al. 2011; Kato and Igarashi 2012). Asano et al. (2011) estimated the centroid moment tensors of earthquakes before and after the 2011 Tohoku-Oki earthquake and revealed that interplate earthquakes did not occur within the large coseismic slip area of this megathrust earthquake, whereas both interplate and non-interplate earthquakes occurred downdip of the large coseismic slip area and along the Japan Trench, as shown in Fig. 1b. Asano et al. (2011) also suggested that the interplate earthquakes that occurred downdip of the coseismic slip area were primarily loaded by coseismic slip and would be promoted by postseismic slip, with normal fault-type

*Correspondence:
Taku Ueda
ueda.taku.24y@st.kyoto-u.ac.jp
[1] Disaster Prevention Research Institute, Kyoto University, Gokasho, Uji, Kyoto 611-0011, Japan
[2] Earthquake Research Institute, The University of Tokyo, 1-1-1 Yayoi, Bunkyo-Ku, Tokyo 113-0032, Japan

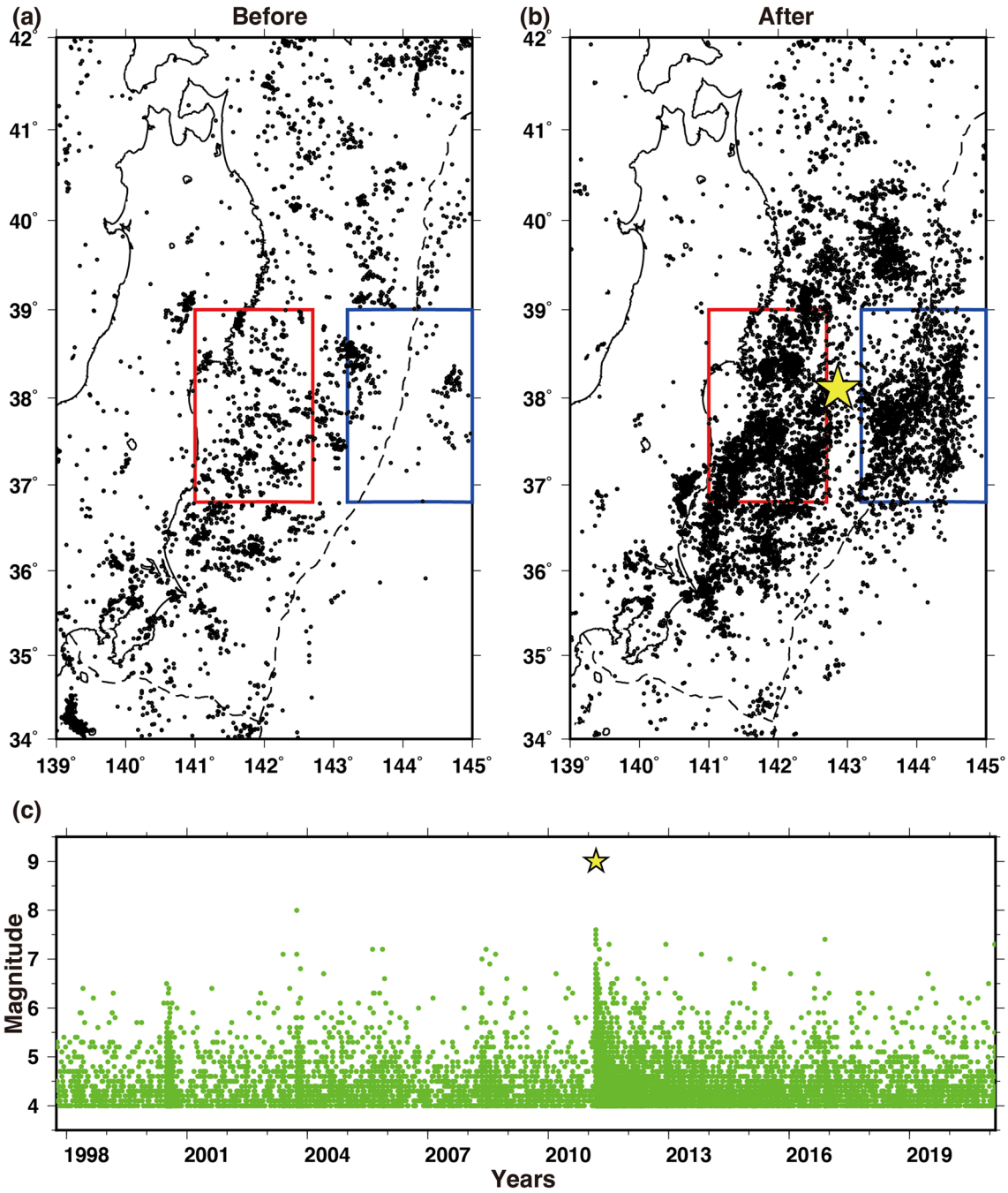

Fig. 1 Epicenter distributions of the detected earthquakes (01/10/1997–20/02/2021) in the study region. **a** Earthquake distribution ($M_j \geq 4.0$, ≤ 100 km depth) before the 2011 Tohoku-Oki earthquake (01/10/1997–11/03/2011). **b** Earthquake distribution ($M_j \geq 4.0$, ≤ 100 km depth) after the 2011 Tohoku-Oki earthquake (11/03/2011–20/02/2021). The yellow star is the epicenter of the 2011 Tohoku-Oki earthquake. Dashed lines denote the trench axes of the Japan Trench and the Sagami Trough. Red and blue rectangular regions denote the downdip and updip regions, respectively, that are mentioned in the discussion. **c** Magnitude–time plot of the earthquakes (01/10/1997–20/02/2021) that occurred in the study region. The $M_j \geq 4.0$ earthquakes are shown in green. The yellow star denotes the 2011 Tohoku-Oki earthquake

aftershocks occurring in the hanging wall owing to tensional stress changes and thrust aftershocks occurring in the footwall owing to compressional stress changes. Very few interplate earthquakes have occurred near the trench and in the outer rise, and the observed normal fault-type aftershocks were activated by tensional stress changes induced by the mainshock rupture (Asano et al. 2011; Obana et al. 2012, 2013).

Various physical models have been suggested to explain the spatiotemporal aftershock distribution of large earthquakes, with most models considering either coseismic stress changes (Dieterich 1994; King et al. 1994; Stein 1999; Toda and Stein 2003, 2022; Kroll et al. 2017; Ozawa and Ando 2021) or afterslip-induced stress loading (Marone et al. 1991; Perfettini and Avouac 2004, 2007; Perfettini et al. 2005; Hsu et al. 2006). However, the contribution of each mechanism to aftershock generation remains unclear. Here we investigate the aftershock generation mechanism following the 2011 Tohoku-Oki earthquake. We first apply the Hierarchical Space–Time Epidemic-Type Aftershock Sequence (HIST-ETAS) model (Ogata et al. 2003; Ogata 2004) to the decade of recorded seismicity since the 2011 Tohoku-Oki earthquake. Using the estimated HIST-ETAS model, we then separate the seismicity into background events (which are generated by either tectonic loading or aseismic phenomena) and triggered events (which are generated by earthquake-to-earthquake interactions). Finally, we discuss the plausible physical processes that generated the aftershocks following this megathrust event based on spatiotemporal variations in the background and triggered events.

2 Methods

We applied the HIST-ETAS model (e.g., Ogata et al. 2003; Ogata 2004; Bansal and Ogata 2013; Ueda et al. 2021) to the observed seismicity rate to investigate spatial variations in the seismicity characteristics and evaluate the probability of a given event being a background event. This model is a point process model that includes the Omori-Utsu law (Utsu 1961; Utsu et al. 1995), which formulates the typical aftershock temporal decay, the Utsu-Seki law (Utsu and Seki 1954), which formulates the relationship between the aftershock area and mainshock magnitude, the decay in aftershock density with distance (e.g., Felzer and Brodsky 2006), and a branching process, such that each earthquake, regardless of magnitude, has the ability to increase the probability of triggering a future earthquake (Iwata 2009).

The earthquake occurrence rate λ at time and location (t, x, y) and occurrence history H_t can be expressed by:

$$\lambda(t,x,y|H_t) = \mu + \sum_{t_i<t} \frac{K}{(t-t_i+c)^p} \left[\frac{(x-x_i, y-y_i) S_i \begin{pmatrix} x-x_i \\ y-y_i \end{pmatrix}}{\exp\{\alpha(M_i - M_c)\}} + d \right]^{-q}, \tag{1}$$

where μ is the background seismicity rate, and the second term expresses the rate of the earthquake occurrence triggered by a magnitude M_i earthquake at time and location (t_i, x_i, y_i), where K, p, and c are the parameters of the Omori-Utsu law, S_i is a non-dimensional positive definite symmetric matrix for anisotropic clusters that is determined by identifying the aftershock cluster using a magnitude-based clustering algorithm (Ogata et al. 1995; Ogata 1998) and then choosing the best-fit ellipsoid that represents the cluster, α is the aftershock magnitude sensitivity, q is the aftershock spatial decay rate, d is a constant, and M_c is the cutoff magnitude, 4.0 in this analysis. We note that H_t includes earthquakes that occurred before the target period (precursory period) because they are potentially influential to the seismicity in the target period (Ogata 2011).

The five seismicity parameters (μ, K, α, p, and q) are given as a function of space and are expressed as:

$$\begin{aligned} \mu(x,y) &= \hat{\mu} \exp\{\vartheta_\mu(x,y)\} \\ K(x,y) &= \hat{K} \exp\{\vartheta_K(x,y)\} \\ \alpha(x,y) &= \hat{\alpha} \exp\{\vartheta_\alpha(x,y)\} \\ p(x,y) &= \hat{p} \exp\{\vartheta_p(x,y)\} \\ q(x,y) &= \hat{q} \exp\{\vartheta_q(x,y)\} \end{aligned}, \tag{2}$$

where $\hat{\mu}$, $\hat{K}$, $\hat{\alpha}$, $\hat{p}$, and $\hat{q}$ correspond to the geometric mean value of each parameter averaged over the analysis region. We adapt each $\vartheta(x,y)$ value to the data by expressing each function using many coefficients that are placed in the locations of each earthquake epicenter and some additional points on the boundary of the analysis region. Each $\vartheta(x,y)$ value at an arbitrary location is linearly interpolated using the three values at the vertices of each Delaunay triangle. The other parameters c and d are location independent.

The unknown parameters can be estimated via the maximum likelihood estimation method. The log-likelihood is expressed as:

$$\log L = \sum_k \log \lambda(t_k, x_k, y_k | H_{t_k}) - \int_0^T \iint_S \lambda(t', x, y | H_{t'}) \mathrm{d}x\mathrm{d}y\mathrm{d}t', \tag{3}$$

where k is the index of each event in the analysis, S is the analysis region, and $[0, T]$ is the analysis interval. However, it is hard to estimate the seismicity parameters stably because the number of unknown parameters is about five times larger than the number of data (events) used in the analysis. We obtained stable solutions by penalizing the spatial gradient of the parameter functions under the assumption of using smoothed functions (the facets of the piecewise linear function being as flat as possible):

$$Q(\theta|\tau) = \sum_{k=1}^{5} w_k \iint_A \left\{ \left(\frac{\partial \vartheta_k}{\partial x}\right)^2 + \left(\frac{\partial \vartheta_k}{\partial y}\right)^2 \right\} \mathrm{d}x\mathrm{d}y, \tag{4}$$

where θ is a set of seismicity parameters, and $\tau = (w_1, \ldots, w_5)$ is a set of weights that is used to tune the strength of the constraints. We then estimated the seismicity parameters that maximized the penalized log likelihood function (Good and Gaskins 1971):

$$R(\theta) = \ln L(\theta) - Q(\theta|\tau). \tag{5}$$

The weights τ were objectively tuned by maximizing the integrated posterior distribution:

$$\Lambda(\tau) = \int_{\Theta} L(\theta)\pi(\theta|\tau)\mathrm{d}\theta, \tag{6}$$

where $\pi(\theta|\tau) \propto \exp\{-Q(\theta|\tau)\}$ is the probability distribution. The solution of θ was then obtained for fixed weights τ by maximizing the penalized log-likelihood in Eq. (5), which yields the optimal maximum a posteriori estimates. See Ogata et al. (2003) and Ogata (2004) for the details of the parameter estimation.

We estimated the uncertainties in the HIST-ETAS parameters at each location following the method outlined in Ueda et al. (2021). We first resampled the data 100 times by randomly extracting 90% of the earthquake data used in this analysis. Note that we did not exclude the M9 mainshock from the resampled data set. We then applied the HIST-ETAS model to each resampled dataset and estimated the spatial patterns of the five seismicity parameters. We note that the reference parameters ($\hat{\mu}$, $\hat{K}$, $\hat{\alpha}$, $\hat{p}$, and $\hat{q}$) may vary significantly among the 100 resampled datasets owing to the trade-offs between each parameter. Herak et al. (2001) investigated the interdependence of the ETAS model parameters using the aftershock sequences of the 1996 Ston-Slano earthquake and highlighted that the degree of correlation can be large, especially for pairs of aftershock parameters. Therefore, we normalized the model parameters by dividing the reference parameters estimated from each resampled dataset and then calculated the standard deviation of $\vartheta(x,y)/\ln 10$ (common logarithm of the normalized parameter) at each location to evaluate the significance of the relative differences in each parameter, independent of the trade-offs between parameters.

We used the JMA unified hypocenter catalog (the preliminary Determination of Epicenters) as the earthquake data in our analysis. We applied the HIST-ETAS model to the $M_{\mathrm{j}} \geq 4.0$ earthquakes that occurred between the timing of the 2011 Tohoku-Oki mainshock (11 March 2011) and 20 February 2021 and were located at ≤ 100 km depth beneath Japan (20–50° N, 120°–150° E). The $M_{\mathrm{j}} \geq 6.0$ earthquakes that occurred since 1922 and the $M_{\mathrm{j}} \geq 4.0$ earthquakes that occurred since February 2011 were used as the precursory occurrence history of the HIST-ETAS model.

3 Results

The spatial distributions of the seismicity parameters that were estimated via the HIST-ETAS model, and their uncertainties are shown in Fig. 2. Here we focus on the spatial variations in the background seismicity rate μ and purified aftershock productivity $K/(c^p d^q)$, which expresses the i-th event's aftershock intensity when and where the i-th event occurs in the Tohoku region (Fig. 2). The background seismicity rate after the 2011 Tohoku-Oki earthquake is low within the large coseismic slip zone (Yokota et al. 2011; Iinuma et al. 2012; Kato and Igarashi 2012), whereas it is high downdip of the large coseismic slip zone along the Pacific coast (Fig. 2a). These spatial differences are significant, given the low uncertainties (Fig. 2c). The purified aftershock productivity after the 2011 Tohoku-Oki earthquake is high around the large coseismic slip area (Fig. 2b). A comparison of the background seismicity rate and purified aftershock productivity suggests that triggered earthquakes have predominantly occurred near the large coseismic slip zone along the Japan Trench, where many aftershocks have occurred (Fig. 1). We don't discuss the other seismicity parameters (e.g., α) because there are no significant spatial variations in these parameters in and around the large coseismic slip zone (Additional file 1: Fig. S1).

4 Discussion

4.1 Spatiotemporal distributions of background and triggered seismicity after the 2011 Tohoku-Oki earthquake

We find a significantly high background seismicity rate downdip of the large coseismic slip zone and relatively high aftershock productivity along the Japan Trench near the large coseismic slip zone compared with the background seismicity rate. Here we discuss the spatiotemporal distributions of the background and triggered seismicity after the 2011 Tohoku-Oki earthquake (Figs. 3, 4 and 5). We evaluate the numbers of background and triggered earthquakes in each 0.1°×0.1° grid by calculating the summation of the probability that each event is classified into a background event and a triggered event, respectively, using the estimated HIST-ETAS parameters. The probability that each event is classified into a background event is explicitly given by Zhuang et al. (2002):

$$\varphi_i = \frac{\mu(x_i, y_i)}{\lambda(t_i, x_i, y_i | H_{t_i})}, \tag{7}$$

(See figure on next page.)

Fig. 2 Spatial distribution of the optimal maximum posterior estimates and their uncertainties of the HIST-ETAS model. **a** Common logarithm of the background seismicity rate μ. **b** Common logarithm of the purified aftershock productivity $K/(c^p d^q)$. **c** Standard deviations of the common logarithm of μ. **d** Standard deviations of the common logarithm of $K/(c^p d^q)$. Black dashed lines denote the Japan Trench axis. Blue solid lines denote the outer edge of the large coseismic slip zone of the 2011 Tohoku-Oki earthquake, as proposed by Kato and Igarashi (2012). Blue dashed and dotted lines denote the iso-slip contours (15-m contour) that were estimated by Iinuma et al. (2012) and Yokota et al. (2011), respectively

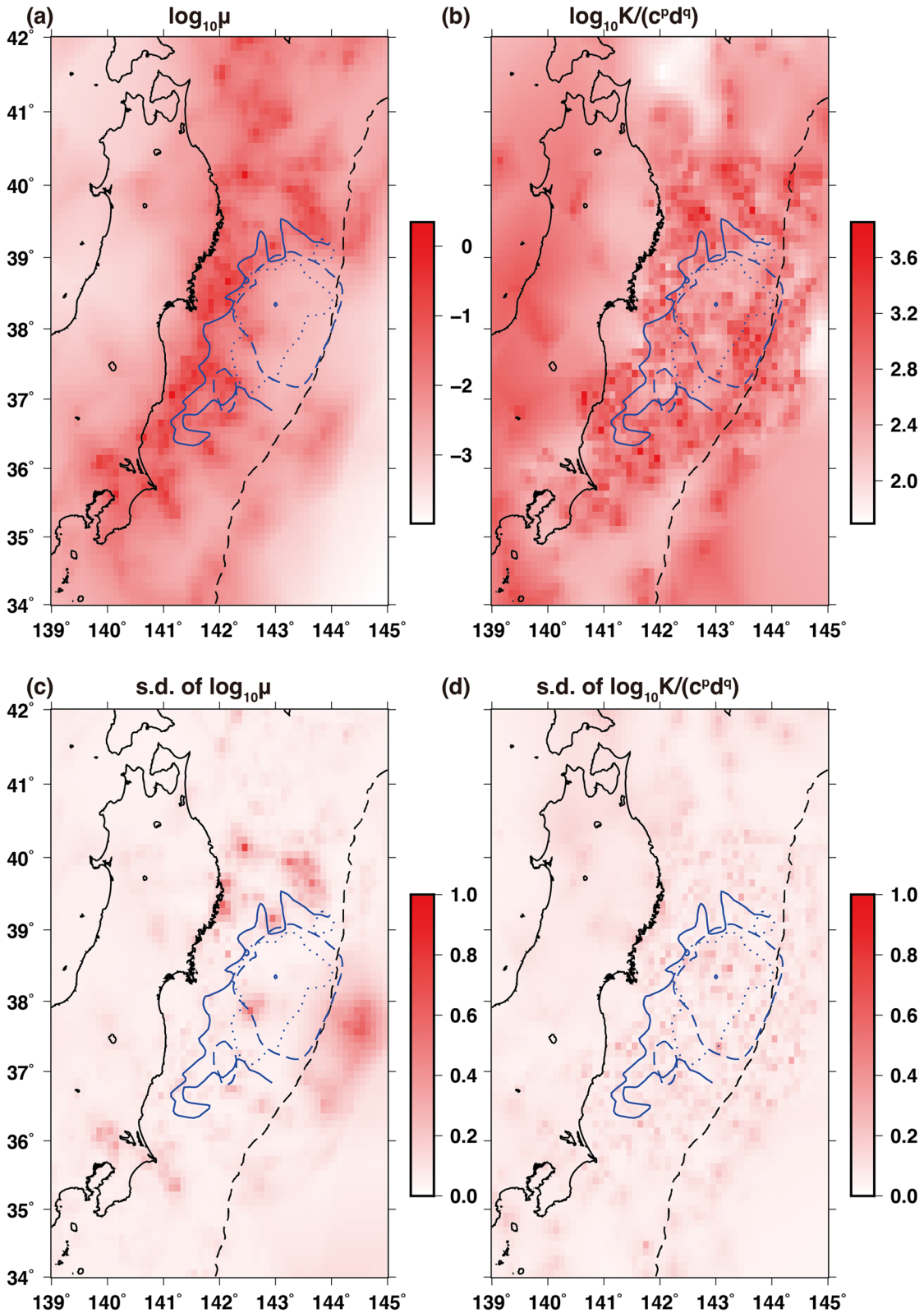

Fig. 2 (See legend on previous page.)

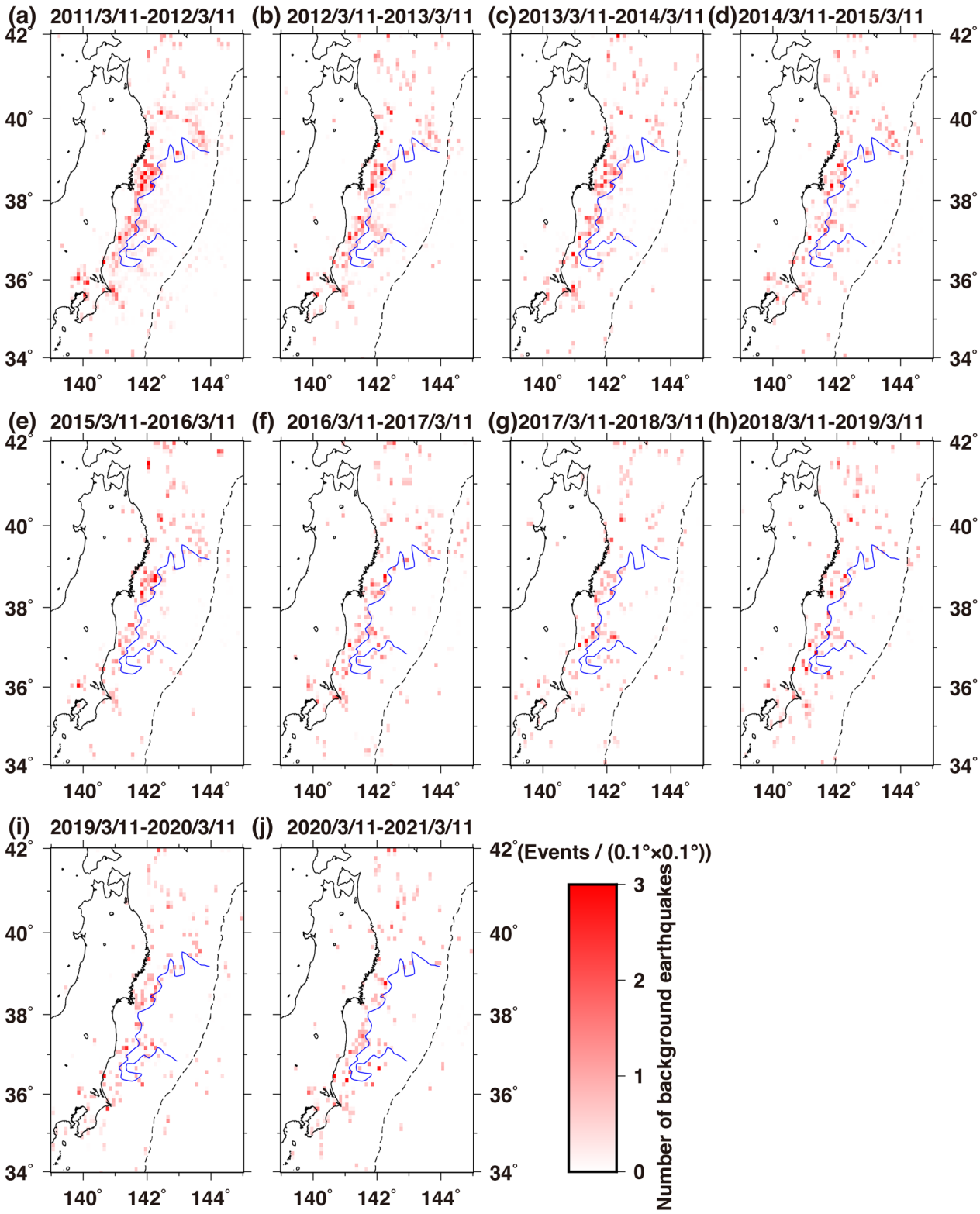

Fig. 3 Spatiotemporal distributions of the number of background earthquakes calculated using the estimated HIST-ETAS model. **a**–**j** Spatial distributions of the number of background earthquakes by year. The black dashed line denotes the Japan Trench axis. The blue solid line denotes the outer edge of the large coseismic slip zone of the 2011 Tohoku-Oki earthquake, as proposed by Kato and Igarashi (2012)

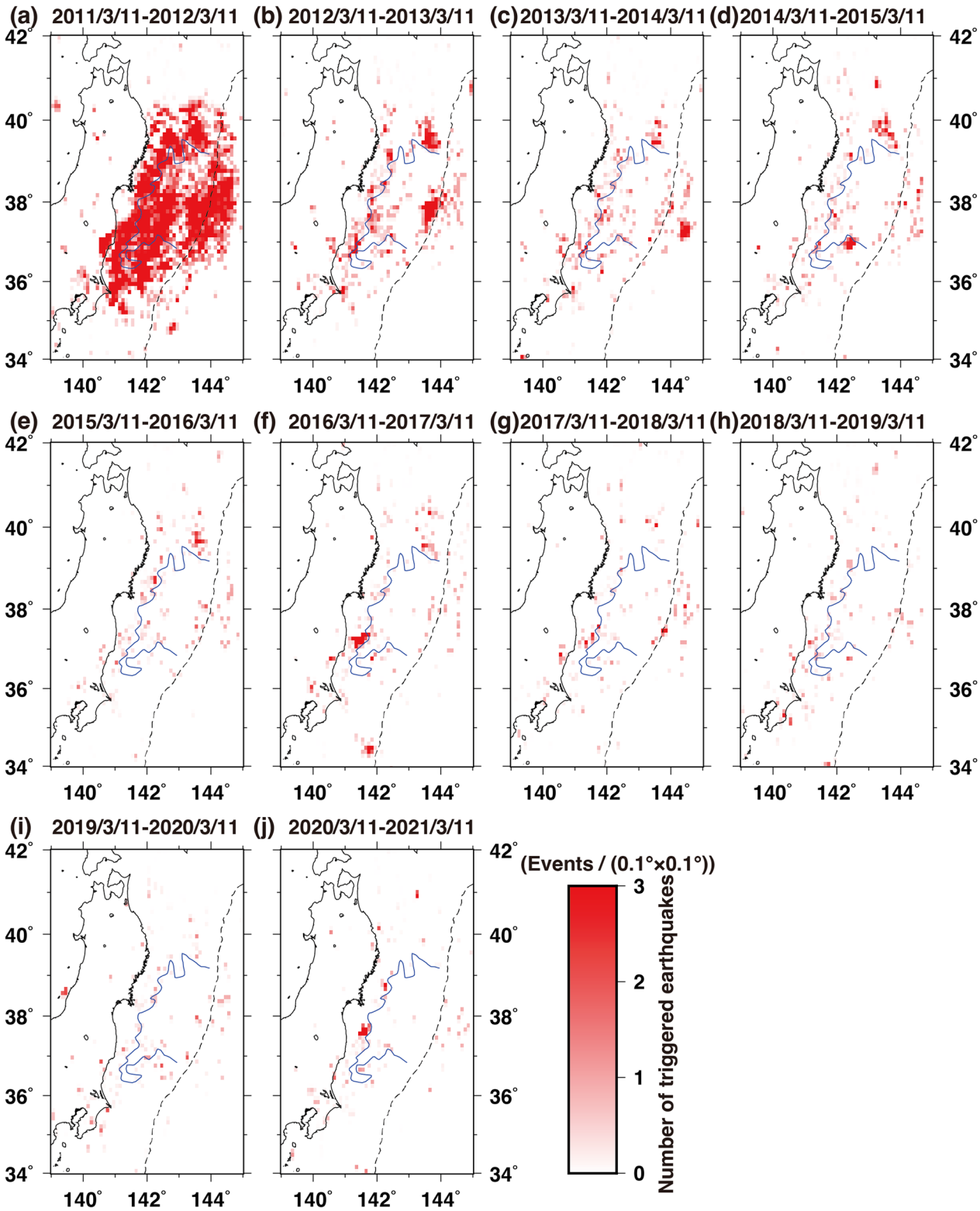

Fig. 4 Spatiotemporal distributions of the number of triggered earthquakes calculated using the estimated HIST-ETAS model. **a**–**j** Spatial distributions of the number of triggered earthquakes by year. Black dashed and blue solid lines are the same as in Fig. 3

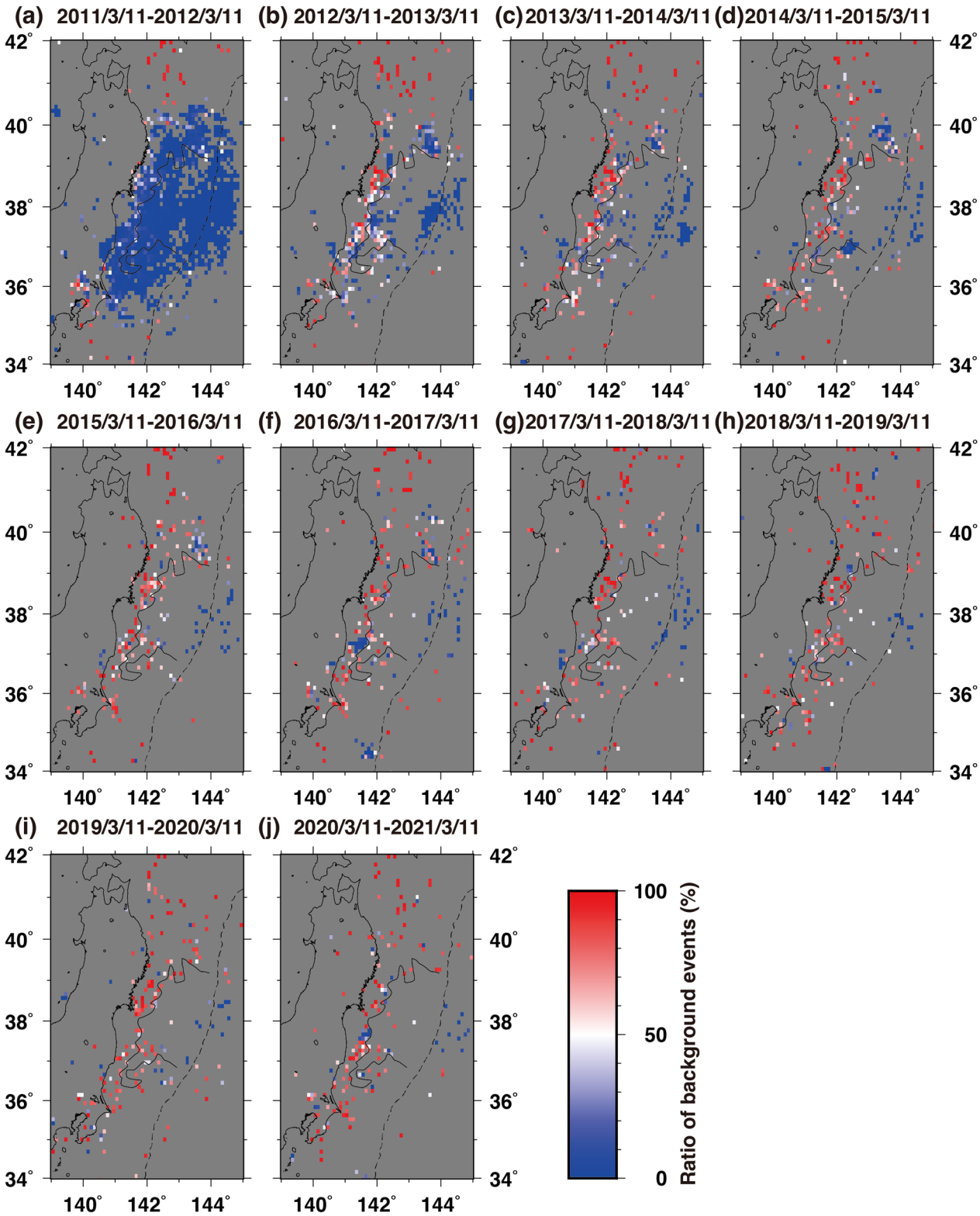

Fig. 5 Spatiotemporal distributions of the ratio of background seismicity to the total seismicity calculated using the estimated HIST-ETAS model. **a**–**j** Spatial distributions of the seismicity ratio by year. Black dashed and solid lines are the same as in Fig. 3

where the numerator and the denominator are the background seismicity rate and total seismicity rate when and where the i-th event occurs, respectively (Eq. 1). The probability that each event is classified into a triggered event is:

$$\rho_i = 1 - \varphi_i. \tag{8}$$

The spatiotemporal distributions of the background and triggered seismicity in the decade since the Tohoku-Oki earthquake (from 11 March 2011 to 11 March 2021) are shown in Figs. 3 and 4, respectively, and the spatiotemporal distribution of the ratio of background events to the total number of earthquakes is shown in Fig. 5. Along the Japan Trench near the large coseismic slip zone, few background earthquakes occurred during the analysis period (Fig. 3), whereas many triggered earthquakes occurred shortly after the 2011 Tohoku-Oki earthquake (Fig. 4a), followed by a decay in triggered seismicity over time (Fig. 4b–j); these spatiotemporal trends were expected based on the background seismicity rate and purified aftershock productivity results (Fig. 2a and b, respectively). The predominance of triggered seismicity relative to background seismicity is further confirmed in Fig. 5, thereby suggesting that the aftershocks along the Japan Trench after the 2011 Tohoku-Oki earthquake are largely due to earthquake-to-earthquake interactions. Many background and triggered earthquakes occurred downdip of the large coseismic slip zone right after the 2011 Tohoku-Oki earthquake (Figs. 3a and 4a), followed by decays in seismicity over time (Figs. 3 and 4). The background earthquakes contributed to the long-term evolution of seismicity following the Tohoku-Oki earthquake (Figs. 3b–j and 5), whereas the triggered seismicity temporarily increased when M7-class earthquakes (e.g., the 2016 and 2021 Fukushima-Oki earthquakes) occurred (Fig. 4f and j). We discuss the factors related to the temporal variations in background seismicity in the following section.

4.2 Relationship between background earthquakes and similar earthquakes downdip of the large coseismic slip zone

Previous studies have discussed the physical processes that control temporal variations in background seismicity (e.g., Hainzl et al. 2013; Kumazawa and Ogata 2013; Kumazawa et al. 2016; Nishikawa and Ide 2017; Nishikawa et al. 2021). Kumazawa and Ogata (2013) evaluated temporal variations in the background seismicity rate of the inland seismicity before and after the 2011 Tohoku-Oki earthquake using the non-stationary ETAS model and attributed the background seismicity rate changes to fluid-based aseismic triggering. Nishikawa and Ide (2017) and Nishikawa et al. (2021) detected earthquake swarms, which yielded sudden increases in the seismicity rate that could not be explained by the aftershock activity, and they suggested that aseismic phenomena, such as slow-slip events, could introduce temporal variations in the background seismicity rate. We compare the spatiotemporal variations in the background seismicity with those of similar earthquakes including repeating earthquakes, which indicate creep movement along the plate interface (Igarashi 2020), to discuss the physical processes that control the spatiotemporal variations in background seismicity downdip of the large coseismic slip zone. The spatial pattern of background seismicity resembles that of the similar earthquakes after the Tohoku-Oki earthquake (Fig. 6). The temporal variability in the number of background earthquakes downdip of the large coseismic slip zone (red rectangular region in Fig. 1) is shown in Fig. 7a, and a clear decay in background seismicity is observed. The relationship between the number of background earthquakes (Fig. 3) and aseismic slip amount, which was calculated using a similar earthquake catalog (Igarashi 2020), is shown in Fig. 7b. We used the method of Uchida et al. (2003) to calculate the aseismic slip amount from the similar earthquake catalog, whereby the slip amount of each similar earthquake is estimated from the following relationship between slip (d; cm) and the seismic moment (M_o; dyne·cm) (Nadeau and Johnson 1998):

$$\log_{10}(d) = -2.36 + 0.17\log_{10}(M_o). \tag{9}$$

The seismic moment for each event is estimated from its magnitude using the following relationship between magnitude and seismic moment (Hanks and Kanamori 1979):

$$\log_{10}(M_o) = 1.5M + 16.1. \tag{10}$$

The temporal variability in the number of background earthquakes closely follows a function of the form $1/t$ (Fig. 7a) and asymptotically approaches the background seismicity rate before the 2011 Tohoku-Oki earthquake, which is roughly estimated from Fig. 3 in Ogata (2011). Note that it will take more time to evaluate at what level the background seismicity will actually settle down to. The number of background earthquakes in each year positively correlates with the aseismic slip amount (Fig. 7b), which suggests that the increase in background seismicity downdip of the large coseismic slip zone is due to the afterslip of the 2011 Tohoku-Oki earthquake, which accumulates linearly with log time (Marone et al. 1991; Perfettini and Avouac 2007).

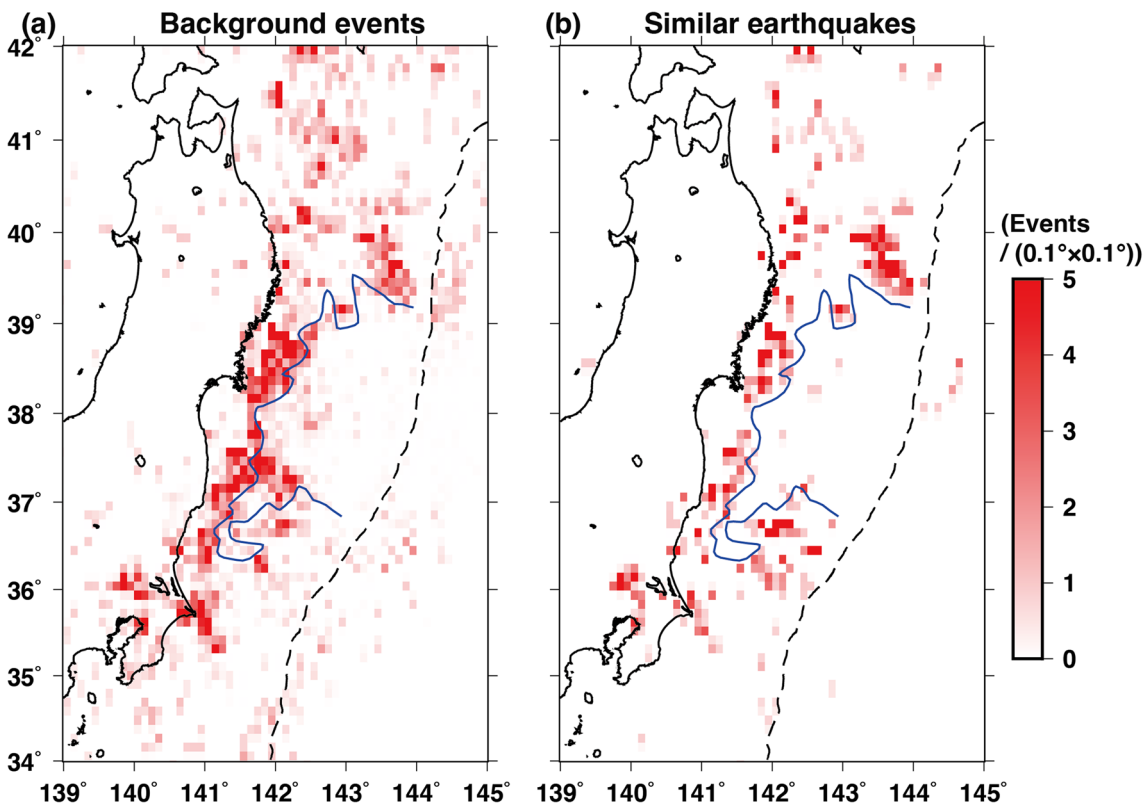

Fig. 6 Spatial distributions of the numbers of background earthquakes and similar earthquakes during the 11/03/2011–11/03/2020 period. **a** Spatial distribution of the number of background earthquakes calculated using the estimated HIST-ETAS model. **b** Spatial distribution of the number of similar earthquakes ($M_j \geq 4.0$) (Igarashi 2020). Black dashed and blue solid lines are the same as in Fig. 3

4.3 Implications for afterslip and aftershocks after the 2011 Tohoku-Oki earthquake

This study suggests that the spatiotemporal variations in the background events are due to the afterslip driven by the 2011 Tohoku-Oki earthquake (Fig. 7). The post-earthquake deformation following the Tohoku-Oki earthquake has been observed using land-based and seafloor geodetic instruments; however, the contributions of viscoelastic relaxation and afterslip to this deformation have been debated (e.g., Fukuda et al. 2013; Sun et al. 2014; Watanabe et al. 2014; Agata et al. 2019; Fukuda and Johnson 2021). Sun et al. (2014) indicated that numerical models of the transient viscoelastic mantle rheology could explain the landward motion of the trench area, thereby suggesting that viscoelastic relaxation plays the dominant role in short-term postseismic deformation, and Fukuda and Johnson (2021) separated the contributions of afterslip and viscoelastic relaxation under the assumption that these mechanisms are driven by coseismic stress changes and interact mechanically with each other to reveal the spatiotemporal afterslip distribution. Figure 7c shows a positive correlation between the number of background earthquakes (Fig. 3) and afterslip (Fukuda and Johnson 2021) averaged downdip of the large coseismic slip zone (red rectangle in Fig. 1). Although it is difficult to separate the contributions of afterslip and viscoelastic relaxation from the geodetic data, our study suggests that the contribution of afterslip can be extracted via a seismicity analysis of the aftershock distribution (Fig. 7).

Although many background and triggered earthquakes have occurred downdip of the large coseismic slip zone, triggered earthquakes were the predominant earthquake type right after the 2011 Tohoku-Oki earthquake (Figs. 3a, 4a, and 5a), thereby suggesting that these earthquakes were caused by the coseismic stress change. This result is consistent with the implication that the aftershocks in the surrounding regions were caused by the stress concentration due to the large coseismic slip (Asano et al. 2011; Kato and Igarashi 2012). Conversely, background earthquakes are the predominant earthquake type in the long term (Figs. 3b–j and 5b–j), and they positively correlate with the aseismic slip amount (Fig. 7b and c), thereby suggesting that temporal variations in the tectonic loading rate (afterslip) have a greater impact on the physical aftershock generation mechanism than the coseismic stress change due to the mainshock

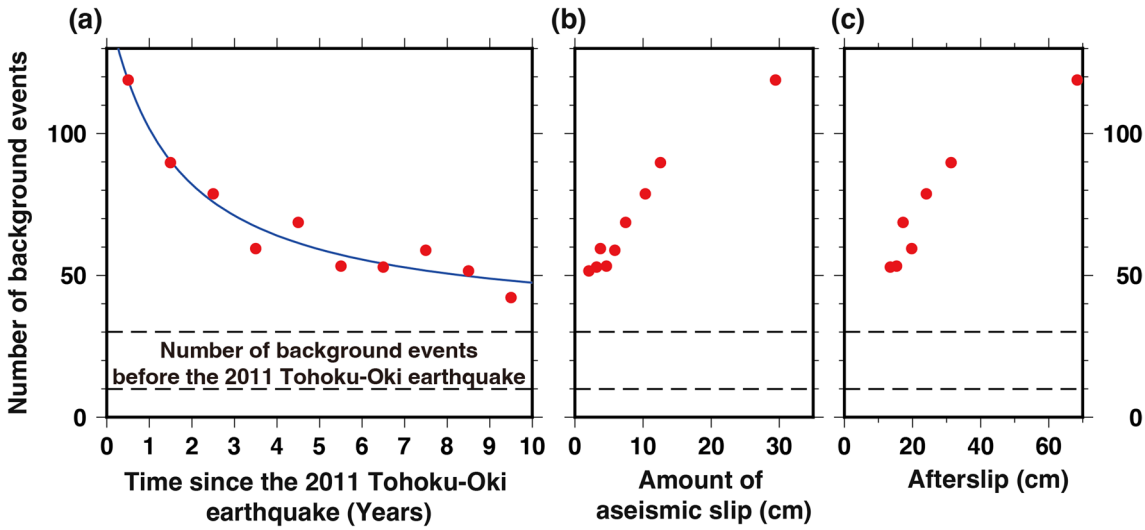

Fig. 7 Temporal variations in the number of background earthquakes compared with the aseismic slip amount. **a** Temporal variations in the number of background earthquakes downdip of the large coseismic slip zone (red rectangle in Fig. 1). The blue curve is the best fit of the function $a + b/(t + c)$ to the observed number of background earthquakes per year (red points). The two black dashed lines provide a possible range for the number of background earthquakes per year before the 2011 Tohoku-Oki earthquake, which is deduced from Fig. 3 in Ogata (2011). **b** Relationship between the number of background earthquakes calculated using the estimated HIST-ETAS model and the aseismic slip amount, which was calculated using the similar earthquake catalog (Igarashi 2020) and the method outlined by Uchida et al. (2003). Black dashed lines are the same as in **a**. **c** Relationship between the number of background earthquakes calculated using the estimated HIST-ETAS model and the afterslip, which was estimated via a geodetic inversion analysis (Fukuda and Johnson 2021). Black dashed lines are the same as in **a**

rupture (Fig. 8). Predominance of triggered earthquakes right after the 2011 Tohoku-Oki earthquake and their faster decay compared with background earthquakes can also be confirmed by temporal variations in background and triggered earthquakes (Additional file 1: Fig. S2).

However, the reverse trend is observed updip of the large coseismic slip zone, as triggered earthquakes are the predominant earthquake type in the long term (Figs. 3, 4, and 5), thereby suggesting that the aftershocks are caused by earthquake-to-earthquake interactions, and that there is a lack of afterslip in this updip region along the Japan Trench (Fig. 8). This result supports previous findings of the normal fault aftershocks in the outer rise potentially being activated by an abrupt increase in extensional stress caused by the mainshock rupture (earthquake-to-earthquake interactions, Asano et al. 2011; Obana et al. 2012, 2013), the lack of afterslip in the updip region (Sun et al. 2014; Agata et al. 2019), and the observation of very few interplate earthquakes in the updip region (Obana et al. 2013, 2021).

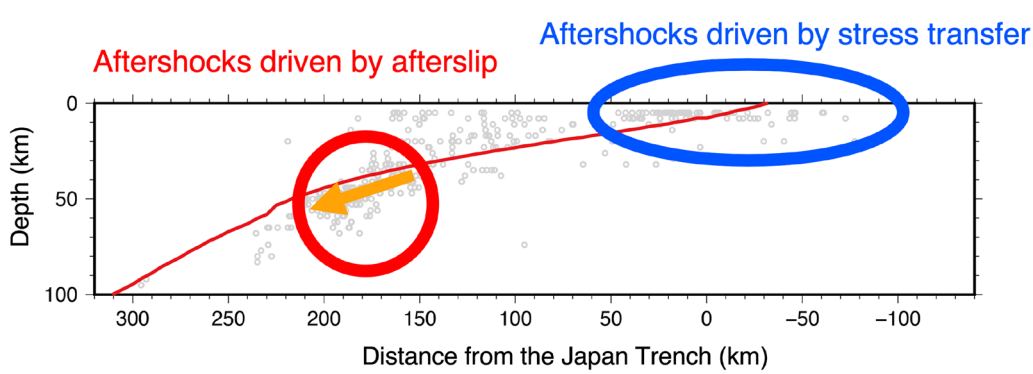

Fig. 8 Interpretation of the aftershock generation mechanisms following the 2011 Tohoku-Oki earthquake. The red line denotes the plate interface (Nakajima and Hasegawa 2006; Kita et al. 2010), and the gray circles are the hypocenters of the events in the F-net hypocenter catalog (11/03/2011–11/03/2021)

4.4 Previous aftershock models

Various physical aftershock models have been proposed to explain aftershock activity, which can be divided into two main categories: static stress changes induced by the mainshock and large aftershocks (Dieterich 1994; King et al. 1994; Stein 1999; Toda and Stein 2003, 2022; Kroll et al. 2017; Ozawa and Ando 2021) and afterslip-induced stress loading (Marone et al. 1991; Perfettini and Avouac 2004, 2007; Perfettini et al. 2005; Hsu et al. 2006). Toda and Stein (2022) forecasted the seismicity changes after the Tohoku-Oki earthquake based on a rate-and-state friction model (Dieterich 1994) that was coupled with Coulomb stress transfer, and they qualitatively explained the quiescence in the mainshock source region and activation in the surrounding area, whereas Perfettini et al. (2019) described the aftershock migration away from the rupture area of the Tohoku-Oki mainshock using an analytical model that was based on afterslip-induced seismicity. Although these studies only considered either mainshock-induced stress changes or afterslip-induced stress loading, our results suggest the importance of considering both mechanisms to explain the aftershock sequence of the 2011 Tohoku-Oki earthquake. Many aftershocks have occurred updip of the large coseismic slip zone along the Japan Trench (blue rectangular region in Fig. 1) without any detectable afterslip (Sun et al. 2014; Agata et al. 2019), whereas the aftershock activity downdip of the large coseismic slip zone (red rectangular region in Fig. 1) has been affected by both mainshock-induced Coulomb stress transfer and afterslip-induced stress loading ((Figs. 3, 4, 5, and 7). Our study successfully divides the aftershocks into background earthquakes, which are inferred to be afterslip-induced events (Fig. 3), and triggered earthquakes, which are inferred to be induced by the stress transfer from other earthquakes (Fig. 4). The present classification is consistent with both the afterslip distribution (Fukuda and Johnson 2021) and mainshock-induced stress change (Asano et al. 2011). Our results suggest that the Coulomb stress model and afterslip model should be combined in future studies to better understand aftershock activity. Furthermore, applying our method to the aftershock sequences of other large earthquakes and quantifying the afterslip-induced seismicity may provide new insights into the relationship between afterslip and aftershocks (Churchill et al. 2022). Our method can be also applied to estimate the afterslip evolution if earthquake catalogs are available, even in areas where geodetic observation networks are sparse. It is therefore possible to employ the classifications using the HIST-ETAS model to advance our understanding of the seismicity characteristics following large earthquakes and to forecast the spatiotemporal evolution of both background and triggered earthquakes. Furthermore, afterslip estimates from earthquake catalogs may motivate the construction of new geodetic observation networks to better observe and quantify aftershock generation mechanisms.

5 Conclusions

We investigated the spatiotemporal characteristics of the aftershocks following the 2011 Tohoku-Oki earthquake by applying the HIST-ETAS model to the decade of recorded seismicity since the mainshock. We successfully divided aftershocks into background earthquakes, which are afterslip-induced events, and triggered events, which are induced by the stress transfer from other earthquakes. Triggered earthquakes are the predominant earthquake type updip of the large coseismic slip zone along the Japan Trench, which is consistent with the lack of afterslip in this region. Background earthquakes are the predominant earthquake type downdip of the large coseismic slip zone, and they positively correlate with the afterslip evolution that was detected using repeating earthquakes and geodetic data. Our results suggest that both stress transfer and afterslip should be considered for both modeling an aftershock sequence and evaluating the relationship between afterslip and aftershocks.

Abbreviations

HIST-ETAS Hierarchical Space–Time Epidemic-Type Aftershock Sequence
JMA Japan Meteorological Agency

Supplementary Information

The online version contains supplementary material available at https://doi.org/10.1186/s40645-023-00564-0.

Additional file 1: Figure S1. Spatial distribution of the optimal maximum posterior estimates and their uncertainties of the HIST-ETAS model.Common logarithm of *a*. Common logarithm of *p*.Standard deviations of the common logarithm of *a*.Standard deviations of the common logarithm of *p*. Black dashed lines denote the Japan Trench axis. Blue solid lines denote the outer edge of the large coseismic slip zone of the 2011 Tohoku-Oki earthquake, as proposed by Kato and Igarashi. Blue dashed and dotted lines denote the iso-slip contoursthat were estimated by Iinuma et al.and Yokota et al., respectively. **Figure S2.** Temporal variations in the number of background and triggered events. Blue circles show temporal variations in the number of triggered events in the red rectangular region in Fig. 1. Red circles show temporal variations in the number of background events in the red rectangular region in Fig. 1.

Acknowledgements

We thank the JMA and NIED for providing the earthquake catalogs. We are grateful to Y. Yokota for providing coseismic slip data for the 2011 Tohoku-Oki earthquake (Yokota et al. 2011) and to J. Fukuda for providing afterslip data for the 2011 Tohoku-Oki earthquake (Fukuda and Johnson 2021). We generated the figures using the Generic Mapping Tools software package (Wessel et al. 2013). We used the computer systems at the Earthquake and Volcano Information Center, the Earthquake Research Institute, the University of Tokyo, Japan, for the presented seismicity analysis. We are grateful to the Editor Y. Yagi and two anonymous reviewers for useful comments. This research is a part of the PhD thesis of Taku Ueda (Ueda 2022).

Author contributions
TU applied the HIST-ETAS model to the earthquake catalog. TU and AK interpreted the results. TU drafted the manuscript. All of the authors read and approved the final manuscript.

Funding
This study was supported by JSPS KAKENHI Grant Numbers 20J11654 and 22J00182. This work was partially supported by JST CREST Grant Number JPMJCR1763.

Availability of data and materials
The JMA and F-net catalogs are available from the NIED (National Research Institute for Earth Science and Disaster Resilience) Data Management Center (https://hinetwww11.bousai.go.jp/auth/?LANG=en and https://www.fnet.bosai.go.jp/event/search.php?LANG=en, respectively). The source codes (FORTRAN) and manual for the HIST-ETAS model can be found in Ogata et al. (2021).

Declarations

Competing interests
The authors declare that they have no competing interests.

Received: 11 February 2023 Accepted: 14 June 2023
Published online: 25 June 2023

References

Agata R, Barbot SD, Fujita K, Hyodo M, Iinuma T, Nakata R, Ichimura T, Hori T (2019) Rapid mantle flow with power-law creep explains deformation after the 2011 Tohoku mega-quake. Nat Commun 10(1):1–4. https://doi.org/10.1038/s41467-019-08984-7

Asano Y, Saito T, Ito Y, Shiomi K, Hirose H, Matsumoto T, Aoi S, Hori S, Sekiguchi S (2011) Spatial distribution and focal mechanisms of aftershocks of the 2011 off the Pacific coast of Tohoku Earthquake. Earth Planets Space 63(7):669–673. https://doi.org/10.5047/eps.2011.06.016

Bansal AR, Ogata Y (2013) A non-stationary epidemic type aftershock sequence model for seismicity prior to the December 26, 2004 M 9.1 Sumatra-Andaman Islands mega-earthquake. J Geophys Res Solid Earth 118(2):616–629. https://doi.org/10.1002/jgrb.50068

Churchill RM, Werner MJ, Biggs J, Fagereng Å (2022) Relative afterslip moment does not correlate with aftershock productivity: Implications for the relationship between afterslip and aftershocks. Geophys Res Lett 49:e2022GL101165. https://doi.org/10.1029/2022GL101165

Dieterich J (1994) A constitutive law for rate of earthquake production and its application to earthquake clustering. J Geophys Res 99(B2):2601–2618. https://doi.org/10.1029/93JB02581

Felzer KR, Brodsky EE (2006) Decay of aftershock density with distance indicates triggering by dynamic stress. Nature 441(7094):735–738. https://doi.org/10.1038/nature04799

Fukuda J, Johnson KM (2021) Bayesian inversion for a stress-driven model of afterslip and viscoelastic relaxation: method and application to postseismic deformation following the 2011 MW 90 Tohoku-Oki earthquake. J Geophys Res Solid Earth 126(5):e2020JB021620. https://doi.org/10.1029/2020JB021620

Fukuda J, Kato A, Kato N, Aoki Y (2013) Are the frictional properties of creeping faults persistent? Evidence from rapid afterslip following the 2011 Tohoku-oki earthquake. Geophys Res Lett 40(14):3613–3617. https://doi.org/10.1002/grl.50713

Good IJ, Gaskins RA (1971) Nonparametric roughness penalties for probability densities. Biometrika 58(2):255–277. https://doi.org/10.1093/biomet/58.2.255

Hainzl S, Ben-Zion Y, Cattania C, Wassermann J (2013) Testing atmospheric and tidal earthquake triggering at Mt. Hochstaufen, Germany. J Geophys Res Solid Earth 118(10):5442–5452. https://doi.org/10.1002/jgrb.50387

Hanks TC, Kanamori H (1979) A moment magnitude scale. J Geophys Res 84(B5):2348–2350

Herak M, Herak D, Markušić S, Ivančić I (2001) Numerical modeling of the Ston-Slano (Croatia) aftershock sequence. Stud Geophys Geod 45(3):251–266. https://doi.org/10.1023/A:1022032128687

Hsu Y-J, Simons M, Avouac J, Galetzka J, Sieh K, Chlieh M, Natawidjaja D, Prawirodirdjo BY (2006) Frictional afterslip following the 2005 Nias-Simeulue earthquake. Sumat Sci 312(5782):1921–1926. https://doi.org/10.1126/science.1126960

Igarashi T (2020) Catalog of small repeating earthquakes for the Japanese Islands. Earth Planets Space 72:73. https://doi.org/10.1186/s40623-020-01205-2

Iinuma T, Hino R, Kido M, Inazu D, Osada Y, Ito Y, Tsushima OM et al (2012) Coseismic slip distribution of the 2011 off the Pacific Coast of Tohoku Earthquake (M90) refined by means of seafloor geodetic data. J Geophys Res Solid Earth 117(7):B07409. https://doi.org/10.1029/2012JB009186

Iwata T (2009) Development of quantitative models representing spatio-temporal distribution of seismicity. Zisin 61:133–141. https://doi.org/10.4294/zisin.61.133

Kato A, Igarashi T (2012) Regional extent of the large coseismic slip zone of the 2011 Mw 9.0 Tohoku-Oki earthquake delineated by on-fault aftershocks. Geophys Res Lett 39(15):L15301. https://doi.org/10.1029/2012GL052220

King GCP, Stein RS, Lin J (1994) Static stress changes and the triggering of earthquakes. Bull Seismol Soc Am 84(3):935–953. https://doi.org/10.1785/BSSA0840030935

Kita S, Okada T, Hasegawa A, Nakajima J, Matsuzawa T (2010) Anomalous deepening of a seismic belt in the upper-plane of the double seismic zone in the Pacific slab beneath the Hokkaido corner: Possible evidence for thermal shielding caused by subducted forearc crust materials. Earth Planet Sci Lett 290(3–4):415–426. https://doi.org/10.1016/j.epsl.2009.12.038

Kroll KA, Richards-Dinger KB, Dieterich JH, Cochran ES (2017) Delayed seismicity rate changes controlled by static stress transfer. J Geophys Res Solid Earth 122(10):7951–7965. https://doi.org/10.1002/2017JB014227

Kumazawa T, Ogata Y (2013) Quantitative description of induced seismic activity before and after the 2011 Tohoku-Oki earthquake by nonstationary ETAS models. J Geophys Res Solid Earth 118(12):6165–6182. https://doi.org/10.1002/2013JB010259

Kumazawa T, Ogata Y, Kimura K, Maeda K, Kobayashi A (2016) Background rates of swarm earthquakes that are synchronized with volumetric strain changes. Earth Planet Sci Lett 442:51–60. https://doi.org/10.1016/j.epsl.2016.02.049

Marone CJ, Scholtz CH, Bilham R (1991) On the mechanics of earthquake afterslip. J Geophys Res 96(B5):8441–8452. https://doi.org/10.1029/91JB00275

Nadeau RM, Johnson LR (1998) Seismological studies at Parkfield VI: moment release rates and estimates of source parameters for small repeating earthquakes. Bull Seismol Soc Am 88(3):790–814. https://doi.org/10.1785/BSSA0880030790

Nakajima J, Hasegawa A (2006) Anomalous low-velocity zone and linear alignment of seismicity along it in the subducted Pacific slab beneath Kanto, Japan: Reactivation of subducted fracture zone? Geophys Res Lett 33(16):L16309. https://doi.org/10.1029/2006GL026773

Nishikawa T, Ide S (2017) Detection of earthquake swarms at subduction zones globally: insights into tectonic controls on swarm activity. J Geophys Res Solid Earth 122(7):5325–5343. https://doi.org/10.1002/2017JB014188

Nishikawa T, Nishimura T, Okada Y (2021) Earthquake swarm detection along the Hikurangi Trench, New Zealand: Insights into the relationship between seismicity and slow slip events. J Geophys Res Solid Earth 126:e2020JB020618. https://doi.org/10.1029/2020JB020618

Obana K, Fujie G et al (2012) Normal-faulting earthquakes beneath the outer slope of the Japan Trench after the 2011 Tohoku earthquake: implications for the stress regime in the incoming Pacific plate. Geophys Res Lett 39(2):L00G24. https://doi.org/10.1029/2011GL050399

Obana K, Kodaira S, Shinohara M, Hino R, Uehira K, Shiobara H, Nakahigashi K, Yamada T, Sugioka H, Ito A, Nakamura Y, Miura S, No T, Takahashi N (2013) Aftershocks near the updip end of the 2011 Tohoku-Oki earthquake. Earth Planet Sci Lett 382:111–116. https://doi.org/10.1016/j.epsl.2013.09.007

Obana K, Fujie G, Yamamoto Y, Kaiho Y, Nakamura Y, Miura S, Kodaira S (2021) Seismicity around the trench axis and outer-rise region of the southern Japan Trench, south of the main rupture area of the 2011 Tohoku-oki

earthquake. Geophys J Int 226(1):131–145. https://doi.org/10.1093/gji/ggab093
Ogata Y (1998) Space-time point-process models for earthquake occurrences. Ann Inst Stat Math 50:379–402. https://doi.org/10.1023/A:1003403601725
Ogata Y (2004) Space-time model for regional seismicity and detection of crustal stress changes. J Geophys Res 109:B03308. https://doi.org/10.1029/2003JB002621
Ogata Y (2011) Significant improvements of the space-time ETAS model for forecasting of accurate baseline seismicity. Earth Planets Space 63(3):217–229. https://doi.org/10.5047/eps.2010.09.001
Ogata Y, Utsu T, Katsura K (1995) Statistical features of foreshocks in comparison with other earthquake clusters. Geophys J Int 121(1):233–254. https://doi.org/10.1111/j.1365-246X.1995.tb03524.x
Ogata Y, Katsura K, Tanemura M (2003) Modelling heterogeneous space-time occurrences of earthquakes and its residual analysis. J R Stat Soc Ser C Appl Stat 52(4):499–509. https://doi.org/10.1111/1467-9876.00420
Ogata Y, Katsura K, Tanemura M, Harte D, Zhuang J (2021) Hierarchical space-time point-process models (HIST-PPM): software documentation and codes. Comput Sci Monogr 35
Ozawa S, Ando R (2021) Mainshock and aftershock sequence simulation in geometrically complex fault zones. J Geophys Res Solid Earth 126(2):e2020JB020865. https://doi.org/10.1029/2020JB020865
Perfettini H, Avouac JP (2004) Postseismic relaxation driven by brittle creep: a possible mechanism to reconcile geodetic measurements and the decay rate of aftershocks, application to the Chi-Chi earthquake. Taiwan J Geophys Res Solid Earth 109(B2):B02304. https://doi.org/10.1029/2003JB002488
Perfettini H, Avouac JP (2007) Modeling afterslip and aftershocks following the 1992 Landers earthquake. J Geophys Res Solid Earth 112(7):B07409. https://doi.org/10.1029/2006JB004399
Perfettini H, Avouac JP, Ruegg JC (2005) Geodetic displacements and aftershocks following the 2001 Mw = 8.4 Peru earthquake: implications for the mechanics of the earthquake cycle along subduction zones. J Geophys Res Solid Earth 110(9):B09404. https://doi.org/10.1029/2004JB003522
Perfettini H, Frank WB, Marsan D, Bouchon M (2019) Updip and along-strike aftershock migration model driven by afterslip: application to the 2011 Tohoku-Oki aftershock sequence. J Geophys Res Solid Earth 124(3):2653–2669. https://doi.org/10.1029/2018JB016490
Stein RS (1999) The role of stress transfer in earthquake occurrence. Nature 402:605–609. https://doi.org/10.1038/45144
Sun T, Wang K, Iinuma T, Hino R, He J, Fujimoto H, Kido M, Osada Y, Miura S, Ohta Y, Hu Y (2014) Prevalence of viscoelastic relaxation after the 2011 Tohoku-oki earthquake. Nature 514(7520):84–87. https://doi.org/10.1038/nature13778
Toda S, Stein R (2003) Toggling of seismicity by the 1997 Kagoshima earthquake couplet: a demonstration of time-dependent stress transfer. J Geophys Res 108(B12):2567. https://doi.org/10.1029/2003JB002527
Toda S, Stein RS (2022) Central shutdown and surrounding activation of aftershocks from megathrust earthquake transfer. Nat Geosci 15:494–500. https://doi.org/10.1038/s41561-022-00954-x
Uchida N, Matsuzawa T, Hasegawa A, Igarashi T (2003) Interplate quasi-static slip off Sanriku, NE Japan, estimated from repeating earthquakes. Geophys Res Lett 30(15):1801. https://doi.org/10.1029/2003GL017452
Ueda T, Kato A, Ogata Y, Yamaya L (2021) Spatial variations in seismicity characteristics in and around the source region of the 2019 Yamagata-Oki Earthquake Japan. Earth Planets Space. https://doi.org/10.1186/s40623-020-01325-9
Ueda T (2022) Seismicity analysis based on statistical modeling: connection with stress change. In: PhD dissertation, The University of Tokyo, Japan
Utsu T (1961) A statistical study on the occurrence of aftershocks. Geophys Mag 30:521–605
Utsu T, Seki A (1954) A relation between the area of aftershock region and the energy of mainshock. Zisin 7:233–240. https://doi.org/10.4294/zisin1948.7.4_233
Utsu T, Ogata Y, Matsu'ura RS, (1995) The centenary of the Omori formula for a decay law of aftershock activity. J Phys Earth 43(1):1–33. https://doi.org/10.4294/jpe1952.43.1
Watanabe SI, Sato M, Fujita M, Ishikawa T, Yokota Y, Ujihara N, Asada A (2014) Evidence of viscoelastic deformation following the 2011 Tohoku-Oki earthquake revealed from seafloor geodetic observation. Geophys Res Lett 41:5789–5796. https://doi.org/10.1002/2014GL061134
Wessel P, Smith WHF, Scharroo R, Luis J, Wobbe F (2013) Generic mapping tools: improved version released. EOS Trans AGU 94(45):409–410
Yokota Y, Koketsu K, Fujii Y, Satake K, Sakai S, Shinohara M, Kanazawa T (2011) Joint inversion of strong motion, teleseismic, geodetic, and tsunami datasets for the rupture process of the 2011 Tohoku earthquake. Geophys Res Lett 38(24):L00G21. https://doi.org/10.1029/2011GL050098
Zhuang J, Ogata Y, Vere-jones D (2002) Stochastic declustering of space-time earthquake occurrences. J Am Stat Assoc 97(458):369–380. https://doi.org/10.1198/016214502760046925

Publisher's Note